Published in final edited form as:
ACS Chem Biol. 2013 June 21; 8(6): 1232–1240. doi:10.1021/cb400027q.

Structural basis for enzyme I inhibition by α-ketoglutarate

Vincenzo Venditti[1], **Rodolfo Ghirlando**[2], and **G. Marius Clore**[1,*]

[1]Laboratorie of Chemical Physics, National Institute of Diabetes and Digestive and Kidney Diseases, National Institutes of Health, Bethesda, Maryland 20892-0520, USA

[2]Laboratorie of Molecular Biology, National Institute of Diabetes and Digestive and Kidney Diseases, National Institutes of Health, Bethesda, Maryland 20892-0520, USA

Abstract

Creating new bacterial strains in which carbon and nitrogen metabolism are uncoupled, is potentially very useful for optimizing yields of microbial produced chemicals from renewable carbon sources. The mechanisms, however, that balance carbon and nitrogen consumption in bacteria are poorly understood. Recently, α-ketoglutarate (αKG), the carbon substrate for ammonia assimilation, has been observed to inhibit *Escherichia coli* enzyme I (EI), the first component of the bacterial phosphotransferase system (PTS), thereby providing a direct biochemical link between central carbon and nitrogen metabolism. Here we investigate the EI-αKG interaction by NMR and enzymatic assays. We show that αKG binds with a $K_D \sim 2.2$ mM at the active site of EI, acting as a competitive inhibitor. In addition, we use molecular docking simulations to derive a structural model of the enzyme-inhibitor complex that is fully consistent with NMR and analytical ultracentrifugation data. We expect that the EI-αKG structure presented here will provide a starting point for structure-based design of EI mutants resistant to αKG.

Introduction

Investigating the mechanisms by which cells integrate information from multiple intra- and extracellular nutrient-sensing pathways is an important aspect of modern biochemistry. In humans, undesired metabolic imbalances can lead to obesity, diabetes and cancer (1,2). In bacteria, efficient reprogramming of metabolic pathways can be exploited to produce valuable products, including biodegradable plastics (3) and biofuels (4–6).

A major contribution to this area of research has recently been provided by Doucette *et al.* (7) who showed that α-ketoglutarate (αKG), the carbon substrate for ammonia assimilation which accumulates in *E. coli* (as well as in other prokaryotic and eukaryotic cells (8)) under conditions of nitrogen limitation, directly blocks glucose uptake across the bacterial membrane by inhibition of enzyme I (EI). Autophosphorylation of EI by phosphoenolpyruvate (PEP) is the first step in the bacterial phosphoenolpyruvate:sugar phosphotransferase system (PTS), a signal transduction pathway in which phosphoryl

*Address correspondence to: G. Marius Clore, Laboratory of Chemical Physics, Building 5, National Institute of Diabetes and Digestive and Kidney Diseases, National Institutes of Health, Bethesda, Maryland 20892-0520, USA. Tel.: 301-496-0788; Fax: 301-496-0825. mariusc@mail.nih.gov.

ASSOCIATED CONTENT

Supporting Information

Analytical ultracentrifugation data for Enzyme I in the presence of phosphoenolpyruvate and α-ketoglutarate, and ^{1}H-^{15}N TROSY correlation spectra of Enzyme I in the presence of various concentrations of α-ketoglutarate. This material is available free of charge via the Internet at http://pubs.acs.org

The authors declare no competing financial interest.

transfer via a series of bimolecular protein-protein interactions is coupled to active transport of sugars across the membrane (9). Inhibition of EI by αKG therefore provides a direct regulatory link between central carbon and nitrogen metabolism in *E. coli*, and represents one of the few documented biochemical mechanisms to date whereby bacterial cells regulate the transport of one elemental nutrient in response to the availability of another. Thus, obtaining structural insights into the inhibition of EI by αKG may serve as a model for more complex cases relevant to eukaryotic biology, and may provide the basis for engineering new bacterial strains in which carbon and nitrogen metabolism are uncoupled. Such strains may be helpful for maximizing the efficiency of microbial overproduction of bioderived molecules where conditions of nitrogen limitation are used to force carbon metabolism into non-physiological pathways (10–12).

Here we present the structural characterization of the EI-αKG interaction. Using biochemical assays and NMR titration experiments, we demonstrate that αKG and PEP compete for the same binding site on the C-terminal domain of EI. On the basis of these results, we use molecular docking simulations to propose a structural model for the EI-αKG complex which is in perfect agreement with the effects of αKG on the NMR spectra and sedimentation properties of EI.

Results and Discussion

NMR spectroscopy

The functional form of EI is a ~128 kDa dimer of identical subunits comprising two structurally and functionally distinct domains connected to one another by a long helical linker (13). The N-terminal domain (EIN, residues 1–249) contains the site of phosphorylation (His^{189}). The C-terminal domain (EIC, residues 261–575) is responsible for dimerization and contains the binding site for PEP. We have investigated the interaction of αKG with the isolated EIN and EIC domains by NMR spectroscopy, and the results are summarized in Figure 1. Addition of 4 mM αKG to the protein samples does not alter the ^{1}H-^{15}N TROSY spectrum of EIN (Figure 1a) but results in substantial changes in the EIC spectrum (Figure 1b), indicating that the EI-αKG interaction occurs exclusively within the C-terminal domain. Analysis of the $^{1}H_N/^{15}N$ chemical shift perturbation ($\Delta_{H/N}$) profile generated by the inhibitor on the combined $^{1}H_N/^{15}N$ chemical shifts of EIC yields an equilibrium dissociation constant (K_D) of ~2.2 ± 0.2 mM for the EI-αKG complex (Figure 1e), which is ~6 times larger than the K_m reported for the EIC-PEP interaction (~0.35 mM (14)). The $\Delta_{H/N}$ profiles at near-saturating concentrations of PEP and αKG are very similar (Figure 1d) with αKG inducing the largest chemical shift perturbations at the binding site for PEP (Figure 1c). These data suggest that PEP and αKG compete for the same binding site on EIC, in contrast with the previously reported noncompetitive mechanism proposed for EI inhibition by αKG (7).

Inhibition assay

To investigate whether αKG affects the stability of the EIC-PEP complex, the ability of EIC to hydrolyze PEP (14) was assayed in the presence of 0, 2 and 4 mM αKG. The resulting kinetic data are reported in Figure 2, and indicate that αKG efficiently inhibits the hydrolytic activity of the enzyme. Fitting the enzymatic data to a competitive inhibition model (eq. 3) yields a K_m of 0.3 ± 0.1 mM and a K_I of 2.2 ± 0.5 mM (Figure 2a), which are in excellent agreement with the K_m value previously reported for the EIC-PEP interaction (14) and with the K_D for the EIC-αKG complex obtained by NMR titration experiments (this work), respectively. In contrast, a much poorer fit is obtained when a non-competitive inhibition model (eq. 4) is used to interpret the enzymatic data (Figure 2b), confirming that formation of the EIC-αKG complex disrupts the interaction of EI with PEP.

The K_m and K_I values (0.3 and 2.2 mM, respectively), which correspond to the equilibrium dissociation constants for the EIC-PEP and EIC-αKG complexes, respectively, were used to calculate the effect of increasing concentrations of αKG on the EI-PEP complex at physiological concentrations of enzyme, substrate and inhibitor. This simulation reveals that 4 mM αKG is sufficient to reduce the percentage of intracellular EI bound to PEP from ~50% to ~25% (Figure 2c), and this value becomes even lower (~15%) when the concentration of αKG reaches 10 mM (which corresponds to the intracellular concentration of αKG measured in *E. coli* cultures grown under nitrogen-poor conditions (7)).

Docking simulation

Taken together, the chemical shift perturbation and enzymatic assay data clearly indicate that PEP and αKG compete for the same binding site on EIC. In addition, the backbone amide ($^1D_{NH}$) residual dipolar couplings (RDCs) measured on samples of weakly aligned EIC and EIC-αKG complex are highly correlated (Figure 1f), indicating the absence of any significant αKG-induced conformational rearrangements in EIC that could result in allosteric disruption of the EIC-PEP interaction. Thus, a structure for the EIC-αKG complex can be obtained by molecular docking of an αKG molecule into the EIC binding site for PEP. Docking simulations with AutoDock 4.0 (33) were performed as described in *Methods*, and the resulting EIC-αKG complex is compared to the EIC-PEP structure in Figure 3. As expected from the close similarity of the chemical structures of the two molecules (Figure 3a), docking results show that PEP and αKG adopt a similar binding mode on EIC. Indeed, for both ligands, the C^1 carboxylic group is involved in hydrogen-bonding interactions with the backbone amides of Asn^{454} and Asp^{455} (Figures 3b,c), while the carbonyl group and the C^5 carboxylic functionality of αKG perfectly overlap with the ethene and phosphoryl groups of PEP, respectively (Figures 3b,c). Interestingly, the docking results also indicate that, although the carbonyl group of αKG is inserted in a small hydrophobic pocket formed by the Leu^{294} and Cys^{502} side chains that accommodates the PEP ethene group in the EI-PEP complex (Figures 3b,c), the hydrophobic penalty engendered by substitution of the CH_2 group by the more polar O atom is compensated by formation of a hydrogen bond between the carbonylic oxygen of αKG and the thiol group of Cys^{502} (Figure 3c). Thus the lower stability of the EI-αKG complex relative to that of EI-PEP must be primarily due to the looser interactions of the αKG C^5 carboxyl group with the side chains of Arg^{296}, Arg^{332}, Lys^{340}, Arg^{358} and Arg^{465} (Figure 3c) that are involved in several hydrogen-bonds and salt-bridges with the PEP phosphoryl group (Figure 3b). In particular, our model shows that the C^5 carboxyl group of αKG forms two hydrogen-bonds with Arg^{465} and is involved in electrostatic interactions with Arg^{358}. In contrast to PEP, however, αKG makes only minor contacts with Arg^{296} and Lys^{340}, and does not interact with the side chain of Arg^{332}.

Validation of the EI-αKG structure

To validate the EI-αKG model obtained by molecular docking simulations, sedimentation velocity experiments were conducted on uniformly $^2H/^{15}N$ labeled EI in the absence and presence of saturating concentrations of PEP and αKG. As previously reported, the specific network of interactions between EI and PEP induces structural stabilization of the EI dimer as well as a ~70° reorientation of EIN domain relative to EIC that results in a more compact enzyme structure (13–15). The sedimentation velocity data reported in Figure 4 reveal that addition of 20 mM PEP or αKG to EI results in a decrease of the EI dimmer dissociation constant by more than an order of magnitude (Figures 4a–c) as well as in a corresponding increase in the sedimentation coefficient extrapolated for the EI dimer ($s_{20,w}$, Figures 4d–e). In particular, $s_{20,w}$ values of 7.77 ± 0.03, 8.09 ± 0.01, and 8.18 ± 0.02 S were obtained for the EI dimer in the free form, and bound to PEP and αKG, respectively, indicating that the PEP-bound structure of EI is more compact than the structure of the free enzyme, and that the αKG-bound form is essentially as compact as the PEP-bound form. The fact that PEP

and αKG have similar effects on both the dimerization properties and the overall shape of EI suggests that the two molecules share a common network of interactions with the enzyme, which is consistent with our model for the EI-αKG complex (Figure 3b,c).

We also noticed that the C^5 carboxyl group of αKG is not a good analog of the PEP phosphoryl group which has a spherically distributed -2*e* charge and is able to form electrostatic interactions with the Mg^{2+} ion and all the positively charged side chains in the EIC active site. Indeed, the C^5 carboxyl group of αKG bears an asymmetric -1*e* charge and is preferentially oriented toward Arg^{465} in our model of the EIC-αKG complex, reproducing only the interactions of PEP with Arg^{358}, Arg^{465} and the Mg^{2+} ion. To verify the existence of this preferential orientation, we compared the NMR data obtained for the EIC-αKG interaction with those previously reported for the EIC-PEP complex (14). NMR chemical shifts are sensitive reporters of the electronic environment surrounding a particular nucleus. Therefore, the observation of a nucleus with similar chemical shifts under different experimental conditions (i.e. in the absence of ligands, in the presence of PEP or αKG) indicates that the local environment surrounding the particular nucleus is unchanged. A perturbation in chemical shift, on the other hand, upon ligand binding is indicative of a change in chemical environment and can be used to reliably identify the site of interaction. Using this basic principle and NMR relaxation dispersion measurements, we have recently shown that the EIC residues around the PEP binding site undergo a rapid transition on the submillisecond time scale between a major open (~97%) and a minor closed (~3%) state (14). Indeed, we have observed a close correspondence between the residue-specific ^{15}N chemical shift differences ($\Delta\omega_N$) between the two states (as derived from analysis of the relaxation dispersion data) and the perturbations on the ^{15}N chemical shifts ($\Delta\delta_N$) of EIC obtained from PEP titration experiments, indicating that the hydrogen bonds and salt bridges formed by the phosphoryl group of PEP with the side chains of Lys^{340}, Arg^{358} and Arg^{465} effectively lock EIC in the closed conformation (14). Good agreement is also obtained by comparing the previously reported $\Delta\omega_N$ values for the open/closed conformational transition (14) with the $\Delta\delta_N$ values measured upon αKG binding (Table 1), with discrepancies higher than 50% of the $\Delta\omega_N$ value observed only in the proximity of Lys^{340} (Figure 3c and Table 1). These observations indicate that αKG is not able to trap Lys^{340} in the closed conformation, and are fully consistent with our structural model of the EIC-αKG complex, in which the C^5 carboxyl group of the inhibitor is involved in strong interactions with Arg^{358} and Arg^{465}, but shows only minor contacts with the Lys^{340} side chain. This preferential orientation of the C^5 carboxyl group is also confirmed by the small $^1H_N/^{15}N$ chemical shift changes for Ile^{275} and Gly^{276} induced by αKG (Figure 1d), in contrast to the large perturbations observed upon addition of PEP (Figure 1d). The amide groups of Ile^{275} and Gly^{276} are indeed located close in space to the side chain of Arg^{296}, that is involved in two hydrogen bonds with the PEP phosphoryl group, but shows only minor contacts with αKG in the proposed structural model (Figures 3b,c). The absence of strong Arg^{296}-αKG interactions leaves the Arg^{296} side chain with the same conformational flexibility as in the free protein. Consequently, the chemical environment of Ile^{275} and Gly^{276} is similar in both free EIC and the EIC-αKG complex, resulting in similar $^1H_N/^{15}N$ chemical shifts (i.e. small $\Delta_{H/N}$ in Figure 1d).

As a final check of the proposed structural model, NMR titration experiments were performed to probe αKG binding to the EIC R465A mutant. Consistent with the disruption of two hydrogen bonds between the C^5 carboxyl group of αKG and the Arg^{465} side chain, the K_D measured for the EIC R465A mutant-αKG complex (~6.7 ± 0.4 mM, Figure 5a) is ~3 times larger than that for the wild-type protein (Figure 1e). As expected, mutation of Arg^{465} also results in destabilization of the enzyme-PEP interaction, evidenced by the higher K_m value (~1.6 ± 0.4 mM) obtained for the EIC R465A mutant-PEP interaction from steady-state enzyme kinetic data (figure 5b).

Concluding remarks

Engineering microorganisms to synthesize bioderived molecules from renewable carbon sources has drawn increasing attention in recent years (16–18). In this context, the use of nitrogen poor culture media has been shown to be advantageous to force carbon into pathways not needed for biomass production (10–12,19). For several practical applications, however, the mechanisms used by microorganisms to balance nutrients run contrary to the metabolic engineers goal of optimizing yields. Thus, in such cases, the use of new microorganisms in which carbon and nitrogen metabolism are uncoupled may be essential for maximizing production rates.

αKG provides the carbon substrate for the glutamine synthetase–glutamate synthase cycle, which assimilates ammonia to produce glutamate. Variations in the concentration of the nitrogen source in the growth medium result in rapid changes in the intracellular concentration of αKG from 0.5 to 10 mM when the nitrogen content of the medium is decreased sufficiently to limit cell growth (7). Interestingly, αKG has been shown in bacteria to link the rate of carbon uptake to the availability of a nitrogen source by inhibition of EI (7), providing an attractive system for synthetic biology studies aimed at engineering new microorganisms with uncoupled carbon and nitrogen metabolism.

Here, we have used NMR to investigate the interaction of αKG with *E. coli* EI. Analysis of the $^{1}H_{N}/^{15}N$ chemical shift profiles generated by αKG on the NMR spectra of the isolated EIN and EIC domains (Figures 1a–d) clearly indicates that αKG interacts exclusively with the C-terminal domain of EI at the binding site for PEP, thus acting as a competitive inhibitor of the enzyme. Although the segment Lys^{250}-Pro^{260} was not included in either of the isolated domain constructs, this fragment comprises a helix connecting the N- and C-terminal domains of the enzyme, does not form pockets, and is not involved in any known interaction with PEP or other molecules. Therefore, the presence of an additional binding site for αKG in the Lys^{250}-Pro^{260} fragment seems very unlikely.

Enzymatic assays performed in the absence and presence of αKG confirm the competitive nature of the inhibition (Figures 2a,b). The K_I of ~2.2 ± 0.5 mM is in excellent agreement with the K_D of the EI-αKG complex measured by NMR titration experiments, and indicates that under conditions of nitrogen limitation the enzyme-inhibitor interaction is strong enough to reduce the percentage of intracellular EI bound to PEP from 50% (at 0 mM αKG) to 15% (at 10 mM αKG) (Figure 2c). Although our results agree well with direct inhibition of EI by αKG, they are inconsistent with the non-competitive inhibition model previously proposed (7). In particular, Doucette *et al.* (7) reported that addition of 2 mM αKG to a reaction mixture containing EI and PEP results in a ~70% reduction in the maximum velocity (V_{max}) for the EI auto-phosphorylation reaction. We note that in our first attempt to titrate αKG (SIGMA – product code: 75892) into EIC we noticed the appearance of several new peaks in the NMR spectra of the protein (Supporting Information, Figure S2), indicative of protein degradation. The degradation was time-dependent, proceeded faster at higher concentration of αKG (Supporting Information, Figure S2), and was not negligible under our experimental conditions (at 4 mM αKG the intensity of the EIC NMR signal dropped more than 60% after 20 min incubation at 37°C). Similar effects were also observed upon titration αKG into the isolated EIN domain, suggesting that our batch of αKG contained a contaminant with high proteolytic activity. Protein degradation in subsequent experiments was eliminated by purchasing a new batch of αKG (SIGMA – product code: K1875 – Premium quality), that was resuspended in the working buffer at a final concentration of 100 mM, checked for pH, aliquoted and immediately frozen. The use of a contaminated batch of αKG for the inhibition assay would result in a reduction in the concentration of active enzyme (that would be quickly proteolyzed by the contaminant) with a concomitant artificial decrease in V_{max}, and may explain the discrepancy between our inhibition data and the ones

previously reported (7). In this respect, we also note that although (i) the NMR data presented here indicate unambiguously that αKG and PEP compete for the same binding site on EIC, (ii) the phosphoryl transfer reaction from PEP bound to the EIC domain to the active site histidine (His189) on the EIN domain is known to occur within the same subunit of the EI dimer (20), and (iii) the structures of both free EI (22) and a phosphoryl transfer intermediate of EI (13) indicate that in-line phosphoryl transfer from EIC of one subunit to EIN of the second subunit within the dimer is sterically impossible, we cannot exclude that binding of αKG to one subunit may induce a conformational change in the relative orientations of the EIN and EIC domains of the second subunit that is incompetent for phosphoryl transfer. In such a case αKG could potentially act as both a competitive and non-competitive inhibitor of EI.

Based on the $^{1}H_{N}/^{15}N$ chemical shift perturbation and enzymatic data that clearly indicated that αKG and PEP compete for the same binding site on EI, we built a model for the EIC-αKG complex by docking an αKG molecule into the binding site for PEP using the molecular docking program AutoDock. Our results indicate that the EIC-αKG complex retains most of the key interactions of the EIC-PEP complex (Figure 3), but with major differences observed at the C^{5} carboxyl group of αKG. In particular the inhibitor makes minimal contacts with the side chains of residues Arg^{296}, Arg^{332} and Lys^{340}, that are involved in an extensive network of electrostatic interactions with the phosphoryl group of PEP. These observations are fully consistent with previously reported NMR relaxation dispersion data (14) and are in good agreement with the effects induced by the inhibitor on the $^{1}H/^{15}N$ chemical shifts (Figure 1d) and on the sedimentation coefficient of the enzyme (Figure 4), confirming that the structural model presented here is of good quality.

Though the competitive nature of the EI inhibition makes the design of EI mutants resistant to αKG non trivial, the fact that the EIC residues involved in PEP binding are fully conserved in the enzyme EI^{NTR} (Figure 6), which catalyzes the same PEP-induced autophosphorylation reaction but is not inhibited by αKG (21), suggests that engineering such EI mutants is not an impossible task. In this respect, the EIC-αKG structure presented here may serve as model for structure-based protein design of EI/EI^{NTR} hybrids that maintain the same enzymatic activity of wild-type EI but are resistant to αKG.

Methods

NMR spectroscopy

The R465A mutant of EIC was created using the QuikChange Site-Directed Mutagenesis Kit (Stratagene). Intact *E. coli* EI (residues 1–575) and the isolated N-terminal (EIN, residues 1–249) and C-terminal (EIC, residues 261–575) domains were expressed and purified as described previously (14,22,23). All NMR samples were prepared in 20 mM Tris buffer, pH 7.4, 100 mM NaCl, 4 mM $MgCl_2$, 1 mM EDTA, 2 mM DTT, and 90% H_2O/10% D_2O (v/v). The protein concentration (in subunits) was 200–400 μM.

NMR spectra were recorded at 37°C on Bruker 600 MHz spectrometers equipped with z-shielded gradient triple resonance cryoprobe. Spectra were processed using NMRPipe (24) and analyzed using the program SPARKY (http://www.cgl.ucsf.edu/ home/sparky).

The ^{1}H-^{15}N TROSY spectra of free EIN and EIC were assigned according to previously reported NMR data (14,25). Assignment of the ^{1}H-^{15}N cross-peaks for the EIC-αKG complex was performed by titration experiments, following the change in ^{1}H-^{15}N cross-peak positions as a function of added αKG in ^{1}H-^{15}N TROSY spectra.

Weighted combined $^{1}H/^{15}N$ chemical shift perturbations ($\Delta_{H/N}$) resulting from the addition of increasing concentrations of αKG (up to 16 mM) were calculated using the equation (26):

$$\Delta_{H/N} = \sqrt{(\Delta\delta_H W_H)^2 + (\Delta\delta_N W_N)^2} \quad (1)$$

where W_H and W_N are weighting factors for the $^{1}H_N$ and ^{15}N amide shifts, respectively ($W_H = 1$, $W_N = 0.154$), and $\Delta\delta_H$ and $\Delta\delta_N$ are the $^{1}H_N$ and ^{15}N chemical shift differences in ppm, respectively, between free and bound states. The dissociation constant (K_D) for the EIC-αKG complex was obtained by fitting the changes in $\Delta_{H/N}$ with increasing concentration of αKG using the following equation (27):

$$\Delta_{H/N} = \Delta_0 \frac{P + L + K_D - \sqrt{(P + L + K_D)^2 - 4PL}}{2P} \quad (2)$$

where Δ_0 is the weighted combined $^{1}H/^{15}N$ chemical shift at saturation, and P and L are the protein and ligand concentrations, respectively. The chemical shift perturbation curves of residues showing $\Delta_{H/N} > 0.1$ ppm in the presence of 16 mM αKG were simultaneously fitted to the same K_D value.

Backbone amide $^{1}D_{NH}$ residual dipolar couplings (RDCs) were measured by taking the difference in $^{1}J_{NH}$ scalar couplings in aligned and isotropic media (28). The alignment media employed was phage *pf1* (14 mg/ml; ASLA Biotech) (29,30), and $^{1}J_{NH}$ couplings were measured using the ARTSY pulse scheme (31).

Enzymatic assay

Enzymatic activity of EIC for the hydrolysis of PEP to inorganic phosphate and pyruvate was assayed spectrophotometrically in the presence of 0, 2 and 4 mM αKG. Assays were performed at 37°C using the EnzChek Phosphate Assay Kit (Invitrogen) and a nanodrop 2000 spectrophotometer, as described previously (14). The experimental enzymatic velocities (v) were fit using either a competitive or a non-competitive inhibition model describing the effect of αKG on the catalytic activity of EIC:

Competitive inhibition:

$$\begin{cases} \nu = \left(\frac{V_{max}[PEP]}{K_m + [PEP]}\right), if\,[\alpha KG] = 0 \\ \nu = \left(\frac{V_{max}[PEP]}{K_m(1 + [\alpha KG]/K_I) + [PEP]}\right), if\,[\alpha KG] > 0 \end{cases} \quad (3)$$

Non-competitive inhibition:

$$\begin{cases} \nu = \left(\frac{V_{max}[PEP]}{K_m + [PEP]}\right), if\,[\alpha KG] = 0 \\ \nu = \left(\frac{V_{max}[PEP]}{(1 + [\alpha KG]/K_I)(K_m + [PEP])}\right), if\,[\alpha KG] > 0 \end{cases} \quad (4)$$

where K_m and V_{max} are the Michaelis constant and maximum velocity in the absence of αKG, respectively, [PEP] and [αKG] are the concentrations of PEP and αKG, respectively, and K_I is the inhibition constant.

The effective Michaelis constant for the EI-PEP complex ($K_{m,eff}$) at αKG concentrations ranging from 0 to 10 mM was calculated using the equation:

$$K_{m,eff} = K_m\,(1 + [\alpha\mathrm{KG}]/K_I) \quad (5)$$

K_m was set to 0.3 mM and K_I to 2.2 mM, as determined by the inhibition assay. The obtained $K_{m,eff}$ values were the used to calculate the percentage of EI bound to PEP at physiological concentrations of enzyme (~10 μM subunits) (32) and PEP (300 μM) (33). Results are presented in Figure 2c.

Docking calculations

The binding mode of αKG to EIC was modeled by docking simulations using the program Autodock 4.0 (34). The coordinates of the C-terminal domain from the phosphorylated EI X-ray structure (13) were used as the target in the docking calculations. A cubic grid box (grid spacing = 0.373 Å; 40 × 40 × 40 grid points) centered on the coordinates of the phosphorylated His^{189} phosphorus atom was used, and the grid maps were generated using the program Autogrid. Docking was performed using the Lamarckian genetic algorithm (LGA) and allowing the side chains of Arg^{332} and Cys^{502} conformational flexibility during the simulations. For αKG, the acrylic and carboxylic group were considered rigid, and only the bonds involving the two sp^3 carbons were treated as rotatable. 100 runs were performed. The population size was set to 150, the maximum number of evaluations to 2,500,000, and the maximum number of generations to 27,000. The remaining parameters were set to their default values. Out of the 100 structures generated, the 10 lowest energy conformations display the same ligand orientation in the binding site. The conformation with the lowest binding energy is displayed in Figure 3c.

Sedimentation velocity

A 1.5 mM stock solution of uniformly $^2H/^{15}N$ labeled EI was diluted to prepare a series of solutions of approximately 130, 65 and 32 μM in 100 mM NaCl, 20 mM Tris buffer, pH 7.4, 4 mM $MgCl_2$, 2 mM DTT and 1 mM EDTA (buffer A). The lowest concentration solution was serially diluted into the same buffer to prepare approximately 2 to 16 μM solutions. All samples were analyzed by sedimentation velocity at 20.0°C and 50 krpm on a Beckman Coulter ProteomeLab XL-I analytical ultracentrifuge. Dilute protein solutions (< 50 μM) were loaded into 12 mm 2-channel epon centerpiece cells (400 μL), whereas higher concentrations were loaded into 3 mm 2-channel epon centerpiece cells (100 μL). Absorbance (280 nm) and Rayleigh interference (655 nm) scans collected at approximately 7 minute intervals were analyzed in SEDFIT 13.0d (35) in terms a continuous *c(s)* distribution covering an *s* range of 0.0 – 10.0 S with a resolution of 200 and a confidence level of 0.68. Good fits were obtained with r.m.s.d. values corresponding to typical instrumental noise values. Identical experiments were carried out in buffer A containing 20 mM PEP (buffer B) or 20 mM αKG (buffer C). The solution density (ρ) and viscosity (η) for buffer A were calculated based on the solvent composition using SEDNTERP 1.09 (36). Solution densities for buffers B and C were measured at 20.000°C on an Anton-Paar DMA 5000 density meter; solution viscosities were measured at 20.00°C using an Anton Paar AMVn rolling ball viscometer. The partial specific volume for EI (*v*) was calculated in SEDNTERP 1.09 (36) and adjusted for its isotopic composition.

EI monomer and dimer populations obtained from integration of the *c(s)* distributions were used to construct partial concentration isotherms. Data were analyzed in SEDPHAT 10.41 (37) in terms of a monomer-dimer self-association to obtain the equilibrium constants; errors were determined using the method of F-statistics with a confidence level of 95%.

Supplementary Material

Refer to Web version on PubMed Central for supplementary material.

Acknowledgments

We thank N. Fawzi and Y. Takayama for helpful discussions. This work was supported by funds from the Intramural Program of the NIH, NIDDK, and the Intramural AIDS Targeted Antiviral Program of the Office of the Director of the NIH (to G.M.C.).

References

1. Guertin DA, Sabatini DM. Defining the role of mTOR in cancer. Cancer Cell. 2007; 12:9–22. [PubMed: 17613433]
2. Kapahi P, Chen D, Rogers AN, Katewa SD, Li PW, Thomas EL, Kockel L. With TOR, less is more: a key role for the conserved nutrient-sensing TOR pathway in aging. Cell Metab. 2010; 11:453–465. [PubMed: 20519118]
3. Anderson AJ, Dawes EA. Occurrence, metabolism, metabolic role, and industrial uses of bacterial polyhydroxyalkanoates. Microbiol Rev. 1990; 54:450–472. [PubMed: 2087222]
4. Wargacki AJ, Leonard E, Win MN, Regitsky DD, Santos CN, Kim PB, Cooper SR, Raisner RM, Herman A, Sivitz AB, Lakshmanaswamy A, Kashiyama Y, Baker D, Yoshikuni Y. An engineered microbial platform for direct biofuel production from brown macroalgae. Science. 2012; 335:308–313. [PubMed: 22267807]
5. Dellomonaco C, Clomburg JM, Miller EN, Gonzalez R. Engineered reversal of the beta-oxidation cycle for the synthesis of fuels and chemicals. Nature. 2011; 476:355–359. [PubMed: 21832992]
6. Bokinsky G, Peralta-Yahya PP, George A, Holmes BM, Steen EJ, Dietrich J, Soon Lee T, Tullman-Ercek D, Voigt CA, Simmons BA, Keasling JD. Synthesis of three advanced biofuels from ionic liquid-pretreated switchgrass using engineered *Escherichia coli*. Proc Natl Acad Sci U S A. 2011; 108:19949–19954. [PubMed: 22123987]
7. Doucette CD, Schwab DJ, Wingreen NS, Rabinowitz JD. α-ketoglutarate coordinates carbon and nitrogen utilization via enzyme I inhibition. Nat Chem Biol. 2011; 7:894–901. [PubMed: 22002719]
8. Boer VM, Crutchfield CA, Bradley PH, Botstein D, Rabinowitz JD. Growth-limiting intracellular metabolites in yeast growing under diverse nutrient limitations. Mol Biol Cell. 2010; 21:198–211. [PubMed: 19889834]
9. Meadow ND, Fox DK, Roseman S. The bacterial phosphoenolpyruvate:glucose phosphotransferase system. Annu Rev Biochem. 1990; 59:497–542. [PubMed: 2197982]
10. Monot F, Engasser JM. Production of acetone and butanol by batch and continuous culture of *Clostridium acetobutylicum* under nitrogen limitation. Biotechnol Lett. 1983; 5:213–218.
11. Kessler B, Weusthuis R, Witholt B, Eggink G. Production of microbial polyesters: fermentation and downstream processes. Adv Biochem Eng Biotechnol. 2001; 71:159–182. [PubMed: 11217411]
12. Aoyama K, Uemura I, Miyake J, Asada Y. Fermentative metabolism to produce hydrogen gas and organic compounds in a cyanobacterium. Spirulina platensis J Ferment Bioeng. 1997; 83:17–20.
13. Teplyakov A, Lim K, Zhu PP, Kapadia G, Chen CC, Schwartz J, Howard A, Reddy PT, Peterkofsky A, Herzberg O. Structure of phosphorylated enzyme I, the phosphoenolpyruvate:sugar phosphotransferase system sugar translocation signal protein. Proc Natl Acad Sci U S A. 2006; 103:16218–16223. [PubMed: 17053069]
14. Venditti V, Clore GM. Conformational selection and substrate binding regulate the monomer/dimer equilibrium of the C-terminal domain of *Escherichia coli* Enzyme I. J Biol Chem. 2012
15. Patel HV, Vyas KA, Savtchenko R, Roseman S. The monomer/dimer transition of enzyme I of the *Escherichia coli* phosphotransferase system. J. Biol. Chem. 2006; 281:17570–17578. [PubMed: 16547355]
16. Steen EJ, Kang Y, Bokinsky G, Hu Z, Schirmer A, McClure A, Del Cardayre SB, Keasling JD. Microbial production of fatty-acid-derived fuels and chemicals from plant biomass. Nature. 2010; 463:559–562. [PubMed: 20111002]

17. Schirmer A, Rude MA, Li X, Popova E, del Cardayre SB. Microbial biosynthesis of alkanes. Science. 2010; 329:559–562. [PubMed: 20671186]
18. Causey TB, Zhou S, Shanmugam KT, Ingram LO. Engineering the metabolism of Escherichia coli W3110 for the conversion of sugar to redox-neutral and oxidized products: homoacetate production. Proc Natl Acad Sci U S A. 2003; 100:825–832. [PubMed: 12556564]
19. Illman AM, Scragg AH, Shales SW. Increase in Chlorella strains calorific values when grown in low nitrogen medium. Enzyme and Microbial Technology. 2000; 27:631–635. [PubMed: 11024528]
20. Navdaeva V, Zurbriggen A, Waltersperger S, Schneider P, Oberholzer AE, Bahler P, Bachler C, Grieder A, Baumann U, Erni B. Phosphoenolpyruvate: sugar phosphotransferase system from the hyperthermophilic Thermoanaerobacter tengcongensis. Biochemistry. 2011; 50:1184–1193. [PubMed: 21250658]
21. Rabus R, Reizer J, Paulsen I, Saier MH. Enzyme INtr from Escherichia coli. J Biol Chem. 1999; 274:26185–26191. [PubMed: 10473571]
22. Schwieters CD, Suh JY, Grishaev A, Ghirlando R, Takayama Y, Clore GM. Solution structure of the 128 kDa enzyme I dimer from Escherichia coli and its 146 kDa complex with HPr using residual dipolar couplings and small- and wide-angle X-ray scattering. J. Am. Chem. Soc. 2010; 132:13026–13045. [PubMed: 20731394]
23. Suh JY, Cai M, Clore GM. Impact of phosphorylation on structure and thermodynamics of the interaction between the N-terminal domain of enzyme I and the histidine phosphocarrier protein of the bacterial phosphotransferase system. J. Biol. Chem. 2008; 283:18980–18989. [PubMed: 18445588]
24. Delaglio F, Grzesiek S, Vuister GW, Zhu G, Pfeifer J, Bax A. NMRPipe: a multidimensional spectral processing system based on UNIX pipes. J. Biomol. NMR. 1995; 6:277–293. [PubMed: 8520220]
25. Garrett DS, Seok YJ, Liao DI, Peterkofsky A, Gronenborn AM, Clore GM. Solution structure of the 30 kDa N-terminal domain of enzyme I of the. *Escherichia coli* phosphoenolpyruvate:sugar phosphotransferase system by multidimensional NMR. Biochemistry. 1997; 36:2517–2530. [PubMed: 9054557]
26. Mulder FA, Schipper D, Bott R, Boelens R. Altered flexibility in the substratebinding site of related native and engineered high-alkaline Bacillus subtilisins. J. Mol. Biol. 1999; 292:111–123. [PubMed: 10493861]
27. Granot J. Determination of dissociation constants of 1:1 complexes from NMR data. Optimization of the experimental setup by statistical analysis of simulated experiments. J Magn Reson. 1983; 55:216–224.
28. Bax A, Kontaxis G, Tjandra N. Dipolar couplings in macromolecular structure determination. Methods Enzymol. 2001; 339:127–174. [PubMed: 11462810]
29. Clore GM, Starich MR, Gronenborn AM. Measurement of residual dipolar couplings of macromolecules aligned in the nematic phase of a colloidal suspension of rodshaped viruses. J. Am. Chem. Soc. 1998; 120:10571–10572.
30. Hansen MR, Mueller L, Pardi A. Tunable alignment of macromolecules by filamentous phage yields dipolar coupling interactions. Nature Struct. Biol. 1998; 5:1065–1074. [PubMed: 9846877]
31. Fitzkee NC, Bax A. Facile measurement of ^{1}H-^{15}N residual dipolar couplings in larger perdeuterated proteins. J. Biomol. NMR. 2011; 48:65–70. [PubMed: 20694505]
32. Rohwer JM, Meadow ND, Roseman S, Westerhoff HV, Postma PW. Understanding glucose transport by the bacterial phosphoenolpyruvate:glycose phosphotransferase system on the basis of kinetic measurements *in vitro*. J. Biol. Chem. 2000; 275:34909–34921. [PubMed: 10889194]
33. Albe KR, Butler MH, Wright BE. Cellular concentrations of enzymes and their substrates. J Theor Biol. 1990; 143:163–195. [PubMed: 2200929]
34. Morris GM, Huey R, Lindstrom W, Sanner MF, Belew RK, Goodsell DS, Olson AJ. AutoDock4 and AutoDockTools4: Automated docking with selective receptor flexibility. J Comput Chem. 2009; 30:2785–2791. [PubMed: 19399780]

35. Schuck P. Size-distribution analysis of macromolecules by sedimentation velocity ultracentrifugation and Lamm equation modeling. Biophys J. 2000; 78:1606–1619. [PubMed: 10692345]

36. Cole JL, Lary JW, T PM, Laue TM. Analytical ultracentrifugation: sedimentation velocity and sedimentation equilibrium. Methods Cell Biol. 2008; 84:143–179. [PubMed: 17964931]

37. Schuck P. On the analysis of protein self-association by sedimentation velocity analytical ultracentrifugation. Anal Biochem. 2003; 320:104–124. [PubMed: 12895474]

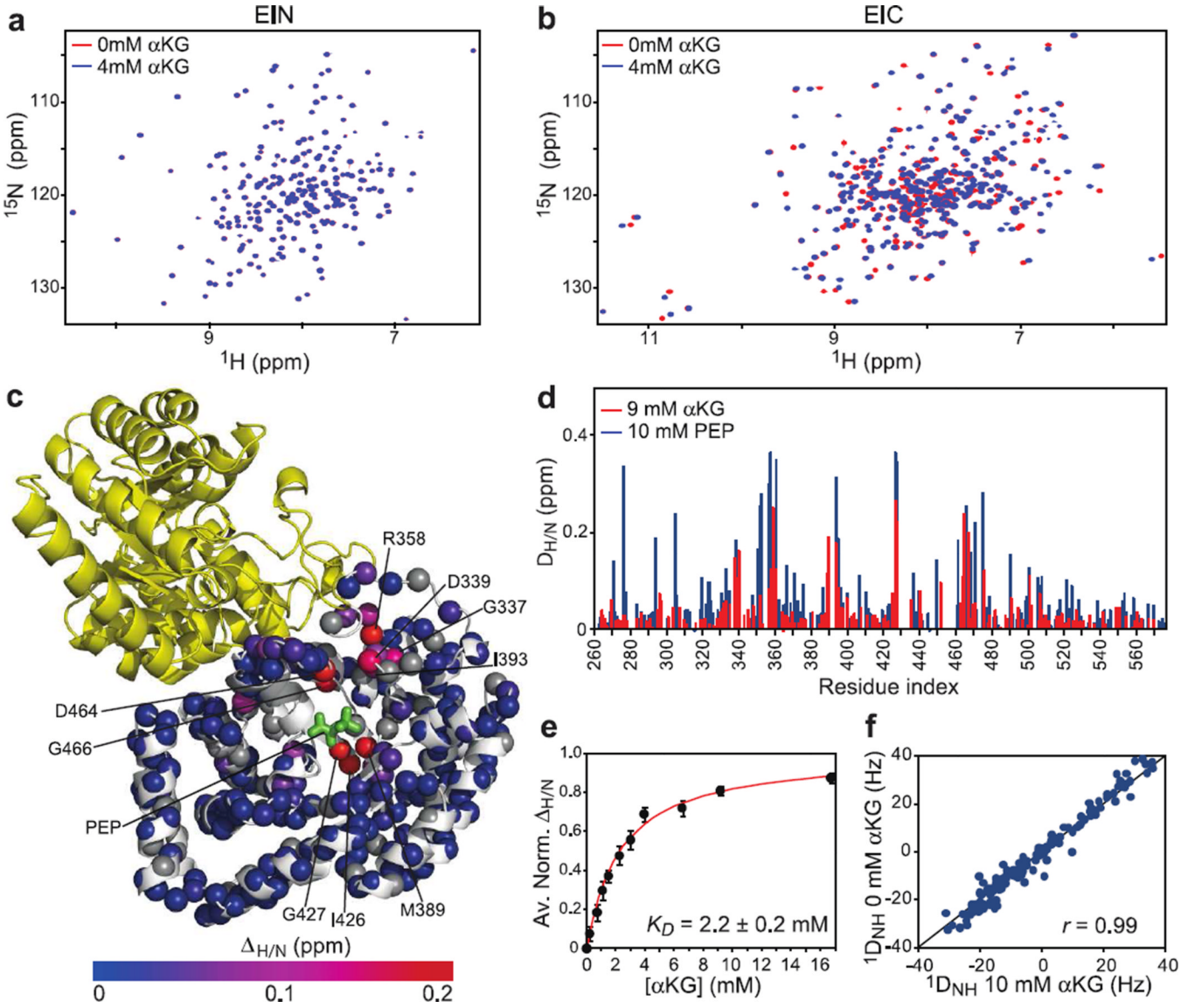

Figure 1. NMR characterization of the EI-αKG interaction

600 MHz ^{1}H-^{15}N TROSY spectra of (**a**) EIN and (**b**) EIC acquired in the absence (*red*) and presence (*blue*) of 4 mM αKG. (**c**) Structural model for the EIC-PEP complex (14) showing the extent of $^{1}H/^{15}N$ chemical shift perturbation ($\Delta_{H/N}$) upon addition of 9 mM αKG to the protein sample. Assigned backbone amides are depicted as spheres and colored according to their $\Delta_{H/N}$ values (color bar ranging from *blue* to *red*). Amide groups assigned only for free EIC are displayed as *grey* spheres. PEP is indicated as *green* bonds. The two subunits of the EIC dimer are colored in *white* and *yellow*. (**d**) Comparison of the $\Delta_{H/N}$ profiles obtained for EIC in the presence of 9 mM αKG (*red*) and 10 mM PEP (14) (*blue*). (**e**) $\Delta_{H/N}$ values as a function of the αKG concentration. Data for all residues showing $\Delta_{H/N} > 0.1$ ppm at 16 mM αKG were simultaneously fit (*red* curve) using a one-site binding model (see *Methods*) yielding a K_D value of 2.2 (±0.2) mM. In the figure, the $\Delta_{H/N}$ were normalized with respect to the fitted $\Delta_{H/N}$ at saturation and averaged over all the residues used in the fitting procedure. The error bars are set to one standard deviation. (**f**) Correlation between the backbone amide RDCs ($^{1}D_{NH}$) measured for EIC in the absence and presence of 10 mM αKG. The high degree of correlation indicate that the orientation of backbone amide bond

vectors relative to the external alignment tensor is unchanged in the two samples showing that binding of αKG does not result in any significant change in backbone conformation.

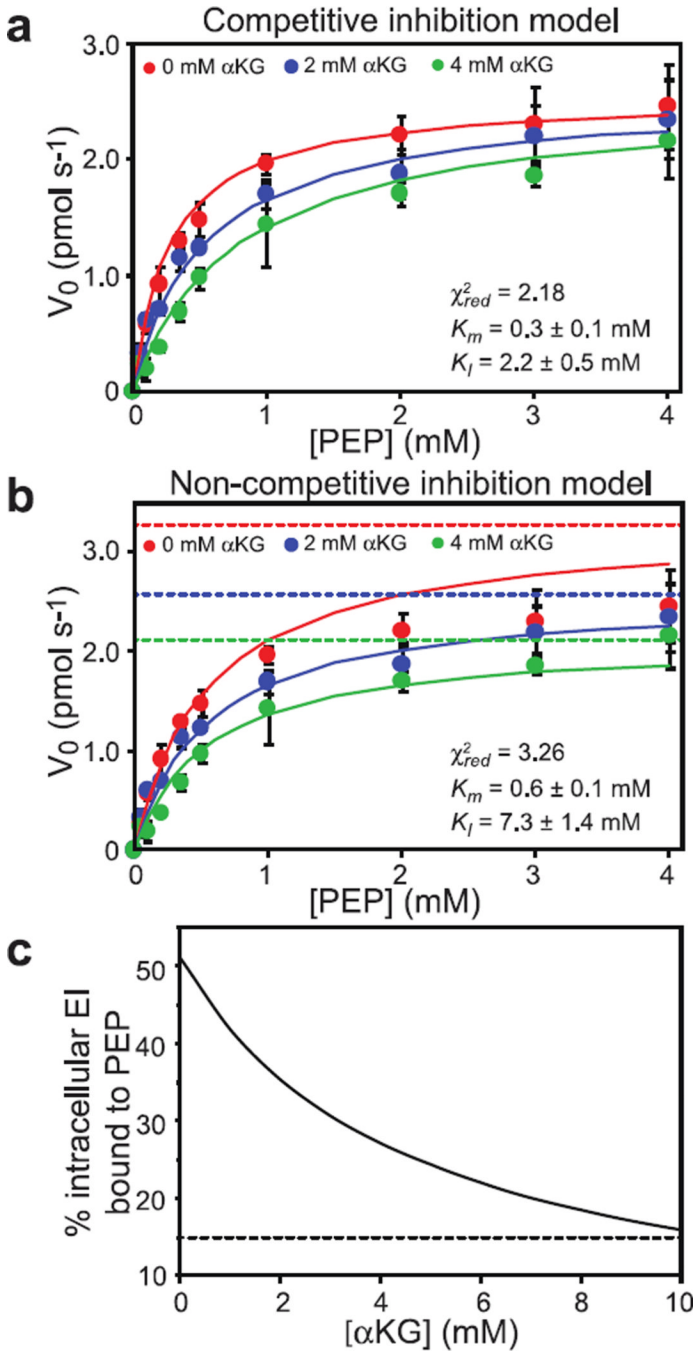

Figure 2. Competitive inhibition of EI by αKG

Michaelis-Menten kinetics for EIC with the substrate PEP. Enzymatic assays were performed in the presence of 0 (*red*), 2 (*blue*) and 4 (*green*) mM αKG. The kinetic data were fitted using competitive (**a**) and non-competitive (**b**) inhibition models. (**c**) Simulation of the percentage of intracellular EI bound to PEP at different concentration of αKG (see *Methods*).

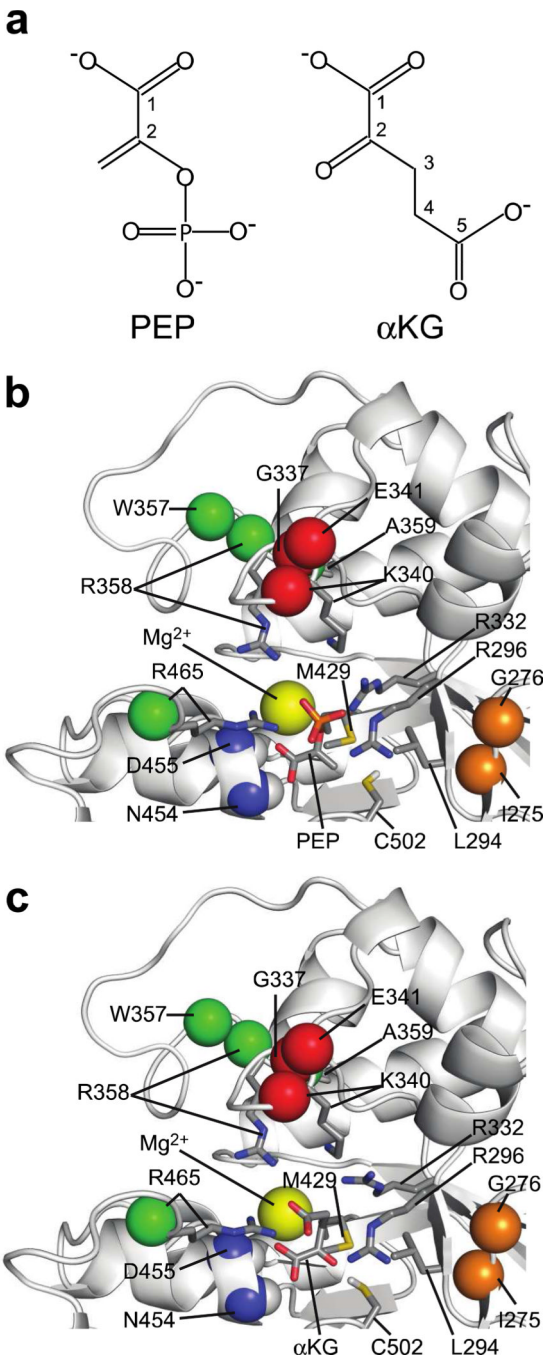

Figure 3. Comparison of PEP and αKG bound in the EIC active site

(**a**) Structures of PEP and αKG. (**b**) and (**c**), Close up views of the EIC active site with bound PEP and αKG, respectively. The Mg^{2+} ion is shown as a *yellow* sphere. The amide groups of Asn^{454} and Asp^{455} are shown as spheres (*blue*; nitrogen; *white*, hydrogen). Side-chains interacting with PEP and αKG are shown as bonds. The Hγ proton of Cys^{502} is indicated in *white* to highlight formation of a hydrogen-bond with the carbonyl group of αKG. The amide groups of Ile^{275} and Gly^{276} are shown as *orange* spheres. Amide groups for which $|(|\Delta\omega_N|-\Delta\delta_N)|/|\Delta\omega_N| > 0.5$ (see Table 1) are shown as *red* spheres (Gly^{337}, Lys^{340},

Glu^{341}). Amide groups for which $|(|\Delta\omega_N|-\Delta\delta_N)|/|\Delta\omega_N| < 0.5$ (see Table 1) are shown as *green* spheres (Trp^{357}, Arg^{358}, Ala^{359}, Arg^{465}).

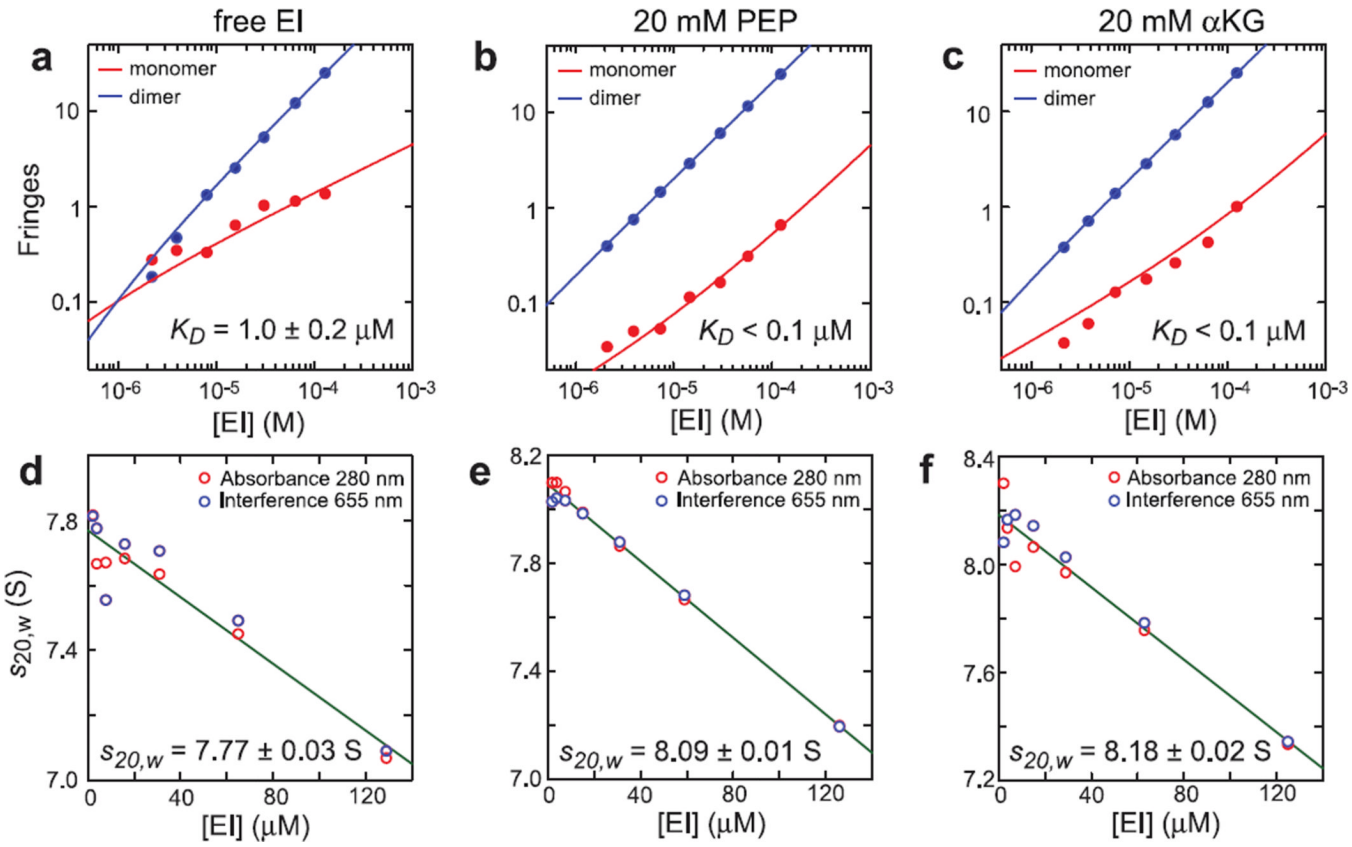

Figure 4. Effect of PEP and αKG on the monomer/dimer equilibrium of EI

(**a–c**), Population isotherms based on sedimentation velocity interference data (Supporting Information, Figure S1) showing the contributions of the EI monomer (*red*) and dimer (*blue*). All signals were normalized to a cell path length of 12 mm. The best fit monomer-dimer equilibrium analysis is depicted by the solid lines. For free EI (**a**) a K_D of 1.0 ± 0.2 μM is obtained, consistent with previous observations (22). In the presence of 20 mM PEP (**b**) and 20 mM αKG (**c**), only traces of monomeric species are detected (Supporting Information, Figure S1). However, the sedimentation velocity data reported in (**b**) and (**c**) can only be fit by assuming that 2.0% of the monomer is incompetent for dimerization, indicating that the monomeric signals detected in (**b**) and (**c**) are due to small amounts of misfolded EI and/or other contaminants. Therefore, in the presence of PEP and αKG EI is essentially entirely dimeric (K_D < 0.1 μM). (**d–f**), Concentration dependence of the EI dimer weight-average sedimentation coefficients obtained from the *c(s)* profiles. S-values at zero concentration were obtained from linear regression and extrapolation to zero concentration. Sedimentation coefficients of 7.77 ± 0.03, 8.09 ± 0.01, and 8.18 ± 0.02 S were determined for the EI dimer in the absence of ligands (**d**), and in the presence of 20 mM PEP (**e**) and 20 mM αKG (**f**), respectively, indicating that the ligand-bound structure of EI is more compact than the structure of the free enzyme, and that the αKG-bound form is essentially as compact as the PEP-bound form.

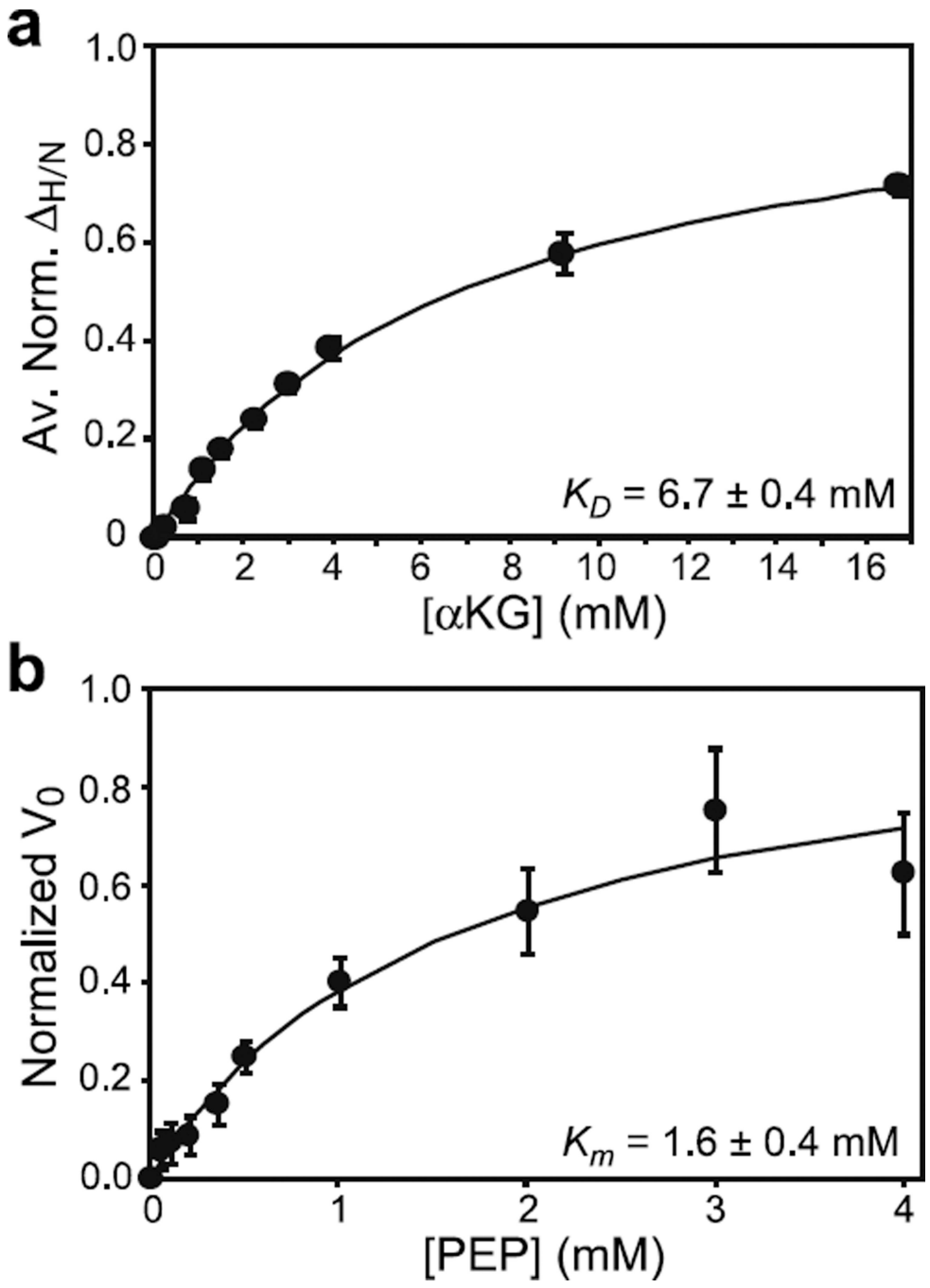

Figure 5. Effect of the active site R465A mutation on the binding of αKG and PEP to EIC

(**a**) Binding of αKG to the R465A EIC mutant as monitored by chemical shift perturbation. Data for all residues showing $\Delta_{H/N}$ > 0.1 ppm at 16 mM αKG were simultaneously fit (solid curve) using a one-site binding model (see *Methods*). In the figure, the $\Delta_{H/N}$ were normalized with respect to the fitted $\Delta_{H/N}$ at saturation and averaged over all the residues used in the fitting procedure. (**b**) Michaelis-Menten kinetics for the R465A EIC mutant with the substrate PEP in the absence of αKG. The error bars are set to one standard deviation.

Figure 6. Sequence alignment of EIC and the C-terminal domain of EI^{NTR} (EIC^{NTR})

The amino acid sequences of EIC and EIC^{NTR} were aligned in BLAST. Exactly conserved residues and conservative mutations are colored *green* and *blue*, respectively. EIC residues involved in the binding with PEP are colored in *red*.

Table 1

Comparison between the chemical shift parameters ($\Delta\omega_N$) for the open/closed conformational exchange of EIC obtained by NMR relaxation dispersion experiments (14), and ^{15}N chemical shift perturbations ($\Delta\delta_N$) induced by αKG on the NMR spectrum of EIC.

	G337	K340	E341	L355	W357	R358	A359	I426	G427	R465	N467
$\lvert\Delta\omega_N\rvert$ (ppm)[a]	2.0	0.6	1.0	1.1	1.0	0.7	2.0	1.9	2.0	0.8	0.8
$\Delta\delta_N$ (ppm)	0.6	0.1	0.4	-	0.7	0.9	1.1	1.6	1.5	1.0	-
$\lvert(\lvert\Delta\omega_N\rvert-\Delta\delta_N)\rvert/\lvert\Delta\omega_N\rvert$	0.7	0.8	0.6	-	0.3	0.3	0.4	0.2	0.3	0.2	-

[a]The error in the values of $\lvert\Delta\omega_N\rvert$ is ±0.1 ppm with the exception of that for Leu^{355} and Arg^{465} which is ±0.2 ppm.